# Favreauite, a new selenite mineral from the El Dragón mine, Bolivia

Stuart J. Mills[1,*], Anthony R. Kampf[2], Andrew G. Christy[3], Robert M. Housley[4], Brent Thorne[5], Yu-Sheng Chen[6] and Ian M. Steele[7]

[1] Geosciences, Museum Victoria, GPO Box 666, Melbourne 3001, Victoria, Australia
*Corresponding author, e-mail: smills@museum.vic.gov.au
[2] Mineral Sciences Department, Natural History Museum of Los Angeles County, 900 Exposition Boulevard, Los Angeles, CA 90007, USA
[3] Centre for Advanced Microscopy, Australian National University, Canberra, ACT 0200, Australia
[4] Division of Geological and Planetary Sciences, California Institute of Technology, Pasadena, CA 91125, USA
[5] 3898 S Newport Circle, Bountiful, UT 84010, USA
[6] Center for Advanced Radiation Sources, University of Chicago, 5640 S. Ellis Avenue, Chicago, IL 60637–1434, USA
[7] Department of Geophysical Sciences, Center for Advanced Radiation Sources, University of Chicago, 5734 S. Ellis Avenue, Chicago, IL 60637–1434, USA

**Abstract:** Favreauite, ideally $PbBiCu_6O_4(SeO_3)_4(OH) \cdot H_2O$, is a new secondary selenite mineral from the El Dragón mine, Antonio Quijarro Province, Potosí Department, Bolivia. The mineral occurs in vughs in a matrix of (Co, Cu)-rich penroseite, dolomite and goethite. Associated minerals are: ahlfeldite, allophane, calcite, chalcomenite, malachite, molybdomenite and an unnamed Al selenite. Favreauite forms tiny green square tabular crystals, flattened on {001}, up to 0.1 mm on edge and 0.01 mm thick, occurring in subparallel and divergent groups. The Mohs hardness of favreauite is estimated as $\approx 3$; it has perfect cleavage on {001}, an irregular fracture and a vitreous lustre. The calculated density based on the empirical formula is 4.851 g cm$^{-3}$. Favreauite is uniaxial (–), with mean refractive index estimated as 1.854 from the Gladstone–Dale relationship. It is pleochroic in shades of green, $O < E$. Electron microprobe analyses gave the empirical formula $Pb_{0.95}Ca_{0.17}Bi_{0.90}Cu_{5.81}Se_{4.10}O_{16}(OH) \cdot 1H_2O$, based on 18 O $pfu$. The Raman spectrum shows strong $SeO_3$ bands at 847 cm$^{-1}$ ($v_1$), 764 and 795 cm$^{-1}$ ($v_3$), 493 and 542 cm$^{-1}$ ($v_2$), and 320 and 392 cm$^{-1}$ ($v_4$). Favreauite is tetragonal, space group $P4/n$, with the unit-cell parameters: $a = 9.860(4)$ Å, $c = 9.700(5)$ Å, $V = 943.0(9)$ Å$^3$ and $Z = 2$. The eight strongest lines in the X-ray powder diffraction pattern are [$d_{obs}$/Å ($I$) ($hkl$)]: 5.67(100)(111), 3.470(76)(220,202), 3.190(35)(003), 2.961(40)(311,113), 2.709(33)(302,203), 2.632(34)(231,312), 2.247(36)(331,133), and 1.6652(33)(305,513,531). The crystal structure was refined to $R_1 = 0.0329$ for 1354 observed reflections [$F_o > 4\sigma F_o$] and 0.0356 for all 1432 unique reflections. Favreauite is a close structural relative of nabokoite, $KCu_7Te^{4+}O_4(SO_4)_5Cl$, and atlasovite, $KCu_6Fe^{3+}BiO_4(SO_4)_5Cl$. In all cases, oxygen-centred tetrahedra share edges to form corrugated [$Cu_6MO_4$] layers ($M$ = Bi or Te) which can be derived from the framework structure of murdochite, $Pb^{4+}Cu^{2+}_6O_{8-x}(Cl,Br)_{2x}$ by selective deletion of atoms. In favreauite, additional OH and $H_2O$ between the layers are weakly bound to Cu, giving it Jahn-Teller distorted 4 + 2 coordination. The Cu–Bi–O layer is braced by $SeO_3$ pyramids. The $Bi^{3+}$ and interlayer $Pb^{2+}$ form an approximately face-centred cubic array analogous to the $Pb^{4+}$ sites in murdochite. Unlike $Bi^{3+}$, $Pb^{2+}$ is in a site with nonpolar $\bar{4}$ point symmetry, which suppresses the stereoactivity of its lone pair.

**Key-words:** favreauite; nabokoite; murdochite; selenite; crystal structure; anion-centred tetrahedra; synchrotron; El Dragón mine; Bolivia.

## 1. Introduction

The new mineral favreauite occurs at the El Dragón mine, Antonio Quijarro Province, Potosí Department, Bolivia (19°49'15''S, 65°55'0''W). The most detailed description of the El Dragón mine is given by Grundmann *et al.* (1990), while more recent information is provided by Paar *et al.* (2012). The El Dragón mine exploited a telethermal deposit consisting of a single selenide vein hosted by sandstones and shales. The principle ore mineral was krut'aite, $CuSe_2$, varying in composition to penroseite, $NiSe_2$, and also often containing significant amounts of Co. Later solutions rich in Bi, Pb and Hg resulted in the crystallization of phases such as clausthalite, watkinsonite, petrovicite and the recently described mineral eldragónite, $Cu_6BiSe_4(Se_2)$ (Paar *et al.*, 2012). Oxidation produced a wide range of secondary phases, including several rare selenites, one of which is favreauite.

The species is named for Mr Georges Favreau, amateur mineralogist and professional engineer, for his

contributions to mineralogy. Mr Favreau has been involved in the discovery and/or description of 10 new minerals: yvonite (Sarp & Černý, 1998), jacquesdietrichite (Kampf & Favreau, 2004), bouazzerite (Brugger *et al.*, 2007), afmite (Kampf *et al.*, 2011), bariopharmacoalumite (Mills *et al.*, 2011), maghrebite (Meisser *et al.*, 2012), angarfite (Kampf *et al.*, 2012a), omsite (Mills *et al.*, 2012a), forêtite (Mills *et al.*, 2012b) and jasrouxite (Topa *et al.*, 2013). He is also one of the discoverers of favreauite, the other discoverer being one of the co-authors (BT). Mr Favreau was the President of the Association Française de Minéralogie (AFM) between 1993 and 2007, and developed the crystal drawing program, FACES. He is an author of more than 50 scientific publications, and was inducted into the Micromounters' Hall of Fame in 2000. The mineral and name (IMA2014–013) were approved by the IMA–CNMNC prior to publication. One co-type specimen is housed in the Geosciences collections at Museum Victoria, Australia, registration number M53004, and three are deposited in the collections of the Natural History Museum of Los Angeles County, Los Angeles, USA, catalogue numbers 64111 to 64113.

## 2. Occurrence, location and physical and optical properties

The new mineral occurs in vughs in a matrix composed mostly of Co- and Cu-rich penroseite, dolomite and goethite. Other secondary minerals found in direct association with favreauite are: ahlfeldite, allophane, calcite, chalcomenite, malachite, molybdomenite and another new mineral with the composition $Al_2(SeO_3)_3 \cdot 6H_2O$, which is currently under study. Favreauite forms tiny green square tabular crystals, which are flattened on {001}, up to 0.1 mm on edge and 0.01 mm thick (Fig. 1), and occur in subparallel and divergent groups. Crystals are transparent with a vitreous lustre, brittle with an irregular fracture, and have perfect cleavage on {001}. The Mohs' hardness is

estimated to be about 3, based upon behaviour when broken.

The density could not be measured because insufficient material is available for direct measurement and the density exceeds that of available density liquids. The calculated density is 4.851 g cm$^{-3}$, based on the empirical formula. Optically, favreauite crystals are uniaxial (–), and are very slightly pleochroic in green tints, with $O < E$. Due to the very limited amount of material available, the small size of the crystals and the high values of the indices of refraction (1.854 based on the Gladstone–Dale relationship), the measurement of the indices of refraction was impractical.

## 3. Chemical composition

Quantitative chemical analyses (6) of favreauite were carried out using a JEOL8200 electron microprobe (WDS mode, 15 kV, 5 nA and 1 μm beam diameter) at the Division of Geological and Planetary Sciences, California Institute of Technology. Analytical results are given in Table 1. The elements S, Te and Cl were all analysed for, but were found to be below their detection limits. No other elements were detected in EDS analyses on several crystal fragments. There was insufficient material for CHN analyses, so H$_2$O was calculated on the basis of 18 O *apfu* and

Table 1. Analytical data for favreauite.

| Const. | wt% | Range | SD | Standard |
|---|---|---|---|---|
| CaO | 0.64 | 0.58–0.72 | 0.06 | anhydrite |
| CuO | 30.63 | 30.02–31.26 | 0.52 | Cu metal |
| PbO | 14.08 | 13.58–14.50 | 0.33 | galena |
| Bi$_2$O$_3$ | 13.95 | 13.71–14.22 | 0.21 | Bi metal |
| SeO$_2$ | 30.16 | 29.35–31.29 | 0.83 | Se metal |
| H$_2$O$_{calc}$ | 1.79 | | | |
| Total | 91.25 | | | |



Fig. 1. Raman spectrum of favreauite.

charge balance. Note that favreauite is prone to electron beam damage (even using the relatively mild conditions noted above), which contributes to the low analytical total.

The empirical formula for favreauite (based on 18 O *apfu*) is: $Pb_{0.95}Ca_{0.17}Bi_{0.90}Cu_{5.81}Se_{4.10}O_{15.96}(OH)_{1.04}\cdot 1H_2O$. The simplified formula is: $PbBiCu_6O_4(SeO_3)_4(OH)\cdot H_2O$, which requires CuO 33.99, PbO 15.89, $Bi_2O_3$ 16.59, $SeO_2$ 31.60 and $H_2O$ 1.92 wt%, total 100 wt%. Detailed consideration of a disordered part of the crystal structure suggests that the hydroxide is at least partly replaced by species such as $HCO_3^-$, $CO_3^{2-}$ and/or $H_2O$, although these could not be quantified (see below). Hence, the formula may be expressed more completely as $PbBiCu_6O_4(SeO_3)_4(OH,HCO_3,CO_3,H_2O)\cdot H_2O$.

## 4. Raman spectroscopy

Raman spectra were obtained with a Renishaw M-1000 microRaman spectrometer system with a 514.3 nm laser through a 20× objective that produced 2.3 mW on an approximately 4 μm diameter spot on a crystal of favreauite. Twenty five spectra were acquired and corrected for a sloping background. A representative spectrum is shown in Figure 1.

In favreauite, the most intense band is at 847 $cm^{-1}$ and corresponds to the $\nu_1$ symmetric stretching mode for $SeO_3$. Other $SeO_3$ bands occurring at 764 and 795 $cm^{-1}$ can be assigned to $\nu_3$ antisymmetric stretching modes, at 493 and 542 $cm^{-1}$ to $\nu_2$ bending modes, and 320 and 392 $cm^{-1}$ to $\nu_4$ bending modes (Verma, 1999). In the O–H stretching region a broad band is seen at 3525 $cm^{-1}$. An unassigned weak band at 989 $cm^{-1}$ may be due to minor $SeO_4^{2-}$, but may alternatively arise from minor components replacing $OH^-$, along with other weak bands at 1065, 1240 and 1341 $cm^{-1}$ (Fig. 1).

## 5. Powder X-ray diffraction

Powder X-ray diffraction data for favreauite were obtained on a Rigaku R-Axis Rapid II curved–imaging-plate microdiffractometer utilising monochromatised Mo$K_\alpha$ radiation. Observed *d* spacings and intensities were derived by profile fitting using JADE 9.3 software (Materials Data Inc.). Data are given in Table 2. The tetragonal unit-cell

Table 2. Powder X-ray data for favreauite (*d*-spacings in Å), 8 strongest lines in bold face.

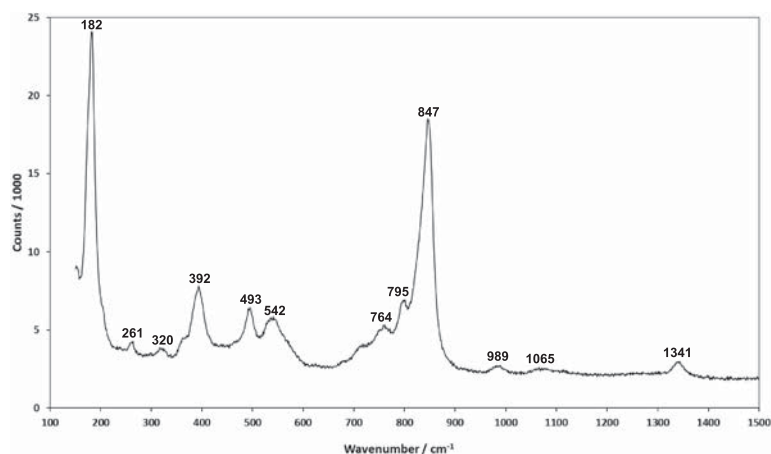| $I_{obs}$ | $d_{obs}$ | $d_{calc}$ | $I_{calc}$ | *hkl* | $I_{obs}$ | $d_{obs}$ | $d_{calc}$ | $I_{calc}$ | *hkl* | $I_{obs}$ | $d_{obs}$ | $d_{calc}$ | $I_{calc}$ | *hkl* |
|---|---|---|---|---|---|---|---|---|---|---|---|---|---|---|
| 7 | 9.81 | 9.7000 | 6 | 0 0 1 | | | 2.1499 | 2 | 2 4 1 | 9 | 1.5938 | 1.5988 | 2 | 6 1 1 |
| 7 | 6.92 | 6.9721 | 1 | 1 1 0 | | | 2.0880 | 2 | 3 2 3 | | | 1.5967 | 1 | 3 5 2 |
| | | 6.9148 | 5 | 1 0 1 | 12 | 1.9951 | 2.0071 | 8 | 4 2 2 | 4 | 1.5567 | 1.5590 | 1 | 6 2 0 |
| **100** | **5.67** | 5.6614 | 100 | 1 1 1 | | | 1.9907 | 3 | 2 2 4 | | | 1.5564 | 1 | 6 0 2 |
| 6 | 4.93 | 4.9300 | 1 | 2 0 0 | 19 | 1.9296 | 1.9337 | 2 | 5 1 0 | | | 1.5392 | 1 | 2 6 1 |
| 5 | 4.35 | 4.3520 | 3 | 1 0 2 | | | 1.9325 | 3 | 4 3 1 | 15 | 1.5237 | 1.5300 | 6 | 5 0 4 |
| 6 | 4.05 | 4.0142 | 4 | 1 2 1 | | | 1.9227 | 4 | 1 4 3 | | | 1.5245 | 3 | 4 0 5 |
| | | 3.9814 | 1 | 1 1 2 | 24 | 1.8885 | 1.8964 | 12 | 1 5 1 | | | 1.5208 | 3 | 5 4 1 |
| **76** | **3.470** | 3.4860 | 30 | 2 2 0 | | | 1.8871 | 10 | 3 3 3 | | | 1.5179 | 3 | 2 1 6 |
| | | 3.4574 | 45 | 2 0 2 | | | 1.8690 | 6 | 1 1 5 | | | 1.4984 | 1 | 3 5 3 |
| 14 | 3.251 | 3.2626 | 8 | 2 1 2 | 9 | 1.8192 | 1.8268 | 3 | 5 0 2 | | | 1.4893 | 1 | 3 3 5 |
| **35** | **3.190** | 3.2333 | 6 | 0 0 3 | | | 1.8216 | 2 | 4 2 3 | 27 | 1.4830 | 1.4842 | 26 | 2 6 2 |
| 28 | 3.113 | 3.1180 | 4 | 3 1 0 | | | 1.8144 | 2 | 2 3 4 | 13 | 1.4648 | 1.4666 | 12 | 2 2 6 |
| | | 3.1128 | 20 | 3 0 1 | | | 1.7992 | 2 | 2 5 1 | | | 1.4612 | 1 | 2 5 4 |
| | | 3.0724 | 3 | 1 0 3 | | | 1.7962 | 1 | 5 1 2 | 7 | 1.4102 | 1.4153 | 6 | 4 4 4 |
| **40** | **2.961** | 2.9684 | 30 | 3 1 1 | 7 | 1.7788 | 1.7757 | 4 | 2 1 5 | | | 1.4067 | 1 | 3 6 2 |
| | | 2.9333 | 14 | 1 1 3 | 33 | 1.7318 | 1.7430 | 13 | 4 4 0 | | | 1.4043 | 1 | 6 2 3 |
| **68** | **2.831** | 2.8307 | 65 | 2 2 2 | | | 1.7287 | 20 | 4 0 4 | 11 | 1.3834 | 1.3944 | 2 | 5 5 0 |
| **33** | **2.709** | 2.7208 | 7 | 3 0 2 | 18 | 1.7029 | 1.7155 | 2 | 4 4 1 | | | 1.3940 | 1 | 7 0 1 |
| | | 2.7037 | 17 | 2 0 3 | | | 1.7130 | 5 | 2 5 2 | | | 1.3917 | 2 | 3 2 6 |
| **34** | **2.632** | 2.6321 | 30 | 2 3 1 | | | 1.7027 | 3 | 4 1 4 | | | 1.3903 | 1 | 5 4 3 |
| | | 2.6228 | 2 | 3 1 2 | | | 1.6952 | 1 | 2 2 5 | | | 1.3830 | 2 | 5 0 5 |
| 24 | 2.462 | 2.4650 | 24 | 4 0 0 | | | 1.6910 | 1 | 5 3 0 | | | 1.3802 | 7 | 7 1 1 |
| | | 2.4250 | 4 | 0 0 4 | | | 1.6836 | 2 | 5 0 3 | 8 | 1.3676 | 1.3722 | 2 | 1 0 7 |
| | | 2.3891 | 1 | 4 0 1 | | | 1.6779 | 1 | 3 3 4 | | | 1.3696 | 5 | 1 5 5 |
| 24 | 2.368 | 2.3706 | 19 | 2 2 3 | **33** | **1.6652** | 1.6707 | 2 | 3 0 5 | | | 1.3673 | 1 | 4 6 0 |
| | | 2.3548 | 5 | 1 0 4 | | | 1.6659 | 14 | 5 3 1 | | | 1.3591 | 2 | 1 1 7 |
| | | 2.3240 | 1 | 3 3 0 | | | 1.6596 | 11 | 5 1 3 | | | 1.3540 | 1 | 4 6 1 |
| | | 2.3219 | 2 | 1 4 1 | 24 | 1.6451 | 1.6472 | 9 | 1 3 5 | | | 1.3527 | 1 | 7 0 2 |
| 3 | 2.308 | 2.3049 | 3 | 3 0 3 | | | 1.6433 | 3 | 6 0 0 | | | 1.3519 | 2 | 4 0 6 |
| **36** | **2.247** | 2.2601 | 10 | 3 3 1 | | | 1.6403 | 3 | 4 4 2 | 7 | 1.3397 | 1.3414 | 3 | 2 7 1 |
| | | 2.2444 | 25 | 1 3 3 | | | 1.6313 | 3 | 4 2 4 | | | 1.3401 | 2 | 7 1 2 |
| 18 | 2.185 | 2.2048 | 5 | 2 4 0 | 10 | 1.6211 | 1.6202 | 1 | 6 0 1 | | | 1.3316 | 3 | 2 5 5 |
| | | 2.1975 | 5 | 4 0 2 | | | 1.6167 | 4 | 0 0 6 | | | | | |
| | | 2.1760 | 9 | 2 0 4 | | | | | | | | | | |

parameters refined from the powder data using JADE 9.3 with whole-pattern fitting are: $a = 9.860(4)$ Å, $c = 9.700(5)$ Å, $V = 943.0(9)$ Å$^3$ and $Z = 2$, which are in excellent agreement with the single-crystal study below.

## 6. Single–crystal X–ray diffraction

Single–crystal structure data were obtained at ChemMatCARS (CARS = Center for Advanced Radiation Sources) Sector 15 at the Advanced Photon Source, Argonne, IL. The single-crystal data were collected using radiation of wavelength 0.49594 Å. Data were recorded using a Bruker 6000 SMART CCD mounted on a Huber 4-circle diffractometer. Data were integrated and corrected for Lorentz-polarization and background effects using SAINTPLUS; SADABS was used for the empirical absorption correction. The structure was solved by direct methods using SIR2004 (Burla *et al.*, 2005). SHELXL-2013 (Sheldrick, 2008) was used for the refinement of the structure. The final model, with all atoms anisotropically refined, converged to $R_1 = 0.0329$ for 1354 observed reflections [$F_o > 4\sigma F_o$] and 0.0356 for all 1432 unique reflections. Data collection and structure refinement details are provided in Table 3, atom coordinates and displacement parameters in Table 4, selected bond distances in Table 5 and bond valence summations in Table 6.

The crystal structure of favreauite (Fig. 2) is comprised of a corrugated layer of CuO$_4$ squares, decorated by SeO$_3$ triangular pyramids. In the sheet, each O is coordinated to three Cu atoms. Pb, Bi, hydroxide and water fill voids in the structure, with Cu making two additional long bonds to interlayer OH$^-$ and H$_2$O forming typical Jahn-Teller

elongated octahedra. Bi occupies hollows in each Cu–O sheet, and the Pb atoms connect successive sheets. Bi and Pb are both in distorted cubic coordination with four long and four short bonds. However, the distortion patterns are quite different (Fig. 3). The Bi site has point symmetry 4, and all four short Bi–O bonds are on the same side, consistent with the presence of a stereoactive lone pair. In contrast, the Pb site has the non-polar point symmetry $\bar{4}$, and short and long bonds alternate around Pb in a pattern that is inconsistent with lone-pair activity (discussed below).

Only oxygens O1, O2, O3 and O4 are integral components of the Cu–O layer. O5 is pyramidally coordinated by four Cu2 atoms with Cu-O distances of 2.875 Å resulting in a bond valence sum for O5 of only 0.16 valence units (Tables 5–6). It is, therefore, deduced to be a H$_2$O molecule. Relatively short non-bonded distances O5⋯Se = 3.83 Å suggest that there is a weak H-bonding interaction between the hydrogen atoms of H$_2$O and the lone pairs of nearby Se atoms. The O6 and O7 sites presented considerable problems in the refinement, and are discussed below.

## 7. Discussion

### 7.1. Nature of the O6/O7 complex

The partially occupied O6 and O7 sites occur in clusters with O6 at the vertices of a tetrahedron and O7 at the centre. The site scattering factors of both O6 and O7 correspond to 4.8 $e^-$, or 60 % of an oxygen atom, and similar in magnitude to the largest residual maxima and minima in electron density (Table 3). Both O6 and O7 are very far from other atoms. O6 has two distant Cu neighbours, giving it a total bond valence sum of 0.26 v.u (Tables 5–6). Apart from O6, the nearest neighbours to O7 are four Cu1 at 3.486 Å and four Cu2 at 3.391 Å, providing only 0.065 v.u if it is assumed that O7 is also an oxygen. Thus, oxygen atoms on O6 or O7 are very underbonded in the structure as refined. Furthermore, the O6⋯O6 distances are only 1.99–2.22 Å, and O6⋯O7 = 1.27 Å, which implies that it is sterically impossible for more than one site out of each (O6)$_4$O7 cluster to be occupied by oxygen alone: if (O$^{2-}$,OH$^-$,H$_2$O) are the only species present, then the maximum possible site occupancy would be 20–25 %, well below the 60 % observed. Thus, it is likely that a small, highly charged cation can also occupy O7 and bond to more than one oxygen atom on the nearby O6 sites, allowing simultaneous occupation of more than one of the latter, and satisfying the major portion of their bond-valence requirements. A cationic species at O7 would also make it possible to obtain the required –1 net charge on the whole O6/O7 cluster, while having scattering equivalent to 4.8 $e^-$ on all sites. The small O6–O7 distance of 1.27 Å eliminates all candidate cations except C$^{4+}$ or N$^{5+}$; this is a typical length for a carbonate C–O bond, but rather long for N–O of nitrate. The EDS spectrum showed K peaks from C and O; the former was assumed to arise

Table 3. Crystal data and structure refinement for favreauite.

| Simplified formula | PbBiCu$_6$O$_4$(SeO$_3$)$_4$(OH) · H$_2$O |
|---|---|
| Temperature | 100(2) K |
| Wavelength | 0. 49594 Å |
| Space group | $P4/n$ |
| Unit-cell dimensions | $a = 9.860(4)$ Å |
| | $c = 9.700(5)$ Å |
| Volume | 943.0(8) Å$^3$ |
| Z | 2 |
| Absorption coefficient | 31.781 mm$^{-1}$ |
| F(000) | 1270 |
| Theta range for data collection | 2.06 to 20.73° |
| Index ranges | $-14 \leq h \leq 14$, $-13 \leq k \leq 14$, $-13 \leq l \leq 13$ |
| Independent reflections | 20676 [$R_{int} = 0.0571$] |
| Refinement method | Full-matrix least-squares on F$^2$ |
| Data/restraints/parameters | 1432/0/83 |
| Goodness-of-fit on F$^2$ | 1.139 |
| Final R indices [$I > 2\sigma(I)$] | $R_1 = 0.0329$, w$R_2 = 0.0356$ |
| R indices (all data) | $R_1 = 0.0697$, w$R_2 = 0.0710$ |
| Extinction coefficient | 0.0006(3) |
| Largest diff. peak and hole | 4.35 and –4.45 $e$/Å$^3$ |

Table 4. Atom coordinates and displacement parameters ($\text{Å}^2$) for favreauite.

| | $x$ | $y$ | $z$ | $U_{eq}$ | $U_{11}$ | $U_{22}$ | $U_{33}$ | $U_{23}$ | $U_{13}$ | $U_{12}$ |
|---|---|---|---|---|---|---|---|---|---|---|
| Pb1 | 0.75 | 0.25 | 1 | 0.01474(15) | 0.01472(18) | 0.01472(18) | 0.0148(3) | 0 | 0 | 0 |
| Bi2 | 0.75 | 0.75 | 0.51701(5) | 0.00427(13) | 0.00424(15) | 0.00424(15) | 0.0043(2) | 0 | 0 | 0 |
| Se | 0.56624(7) | 0.53945(7) | 0.82772(7) | 0.00979(16) | 0.0105(3) | 0.0104(3) | 0.0084(3) | −0.0009(2) | −0.0003(2) | −0.0047(2) |
| Cu1 | 0.5 | 0.5 | 0.5 | 0.0096(2) | 0.0120(5) | 0.0094(5) | 0.0075(5) | 0.0013(4) | 0.0013(4) | −0.0039(4) |
| Cu2 | 0.73943(9) | 0.51655(9) | 0.27943(9) | 0.01080(19) | 0.0094(4) | 0.0128(4) | 0.0102(4) | −0.0047(3) | 0.0006(3) | −0.0001(3) |
| O1 | 0.6097(5) | 0.6215(5) | 0.3859(5) | 0.0071(8) | 0.007(2) | 0.006(2) | 0.008(2) | −0.0002(16) | −0.0005(16) | −0.0026(16) |
| O2 | 0.3974(5) | 0.5656(6) | 0.8447(6) | 0.0192(12) | 0.007(2) | 0.029(3) | 0.022(3) | −0.012(2) | −0.002(2) | 0.000(2) |
| O3 | 0.6010(7) | 0.5667(7) | 0.6605(6) | 0.0253(14) | 0.026(3) | 0.041(4) | 0.008(2) | 0.007(2) | 0.000(2) | −0.024(3) |
| O4 | 0.5787(6) | 0.3661(6) | 0.8419(6) | 0.0183(11) | 0.021(3) | 0.014(3) | 0.019(3) | 0.000(2) | −0.015(2) | −0.001(2) |
| O5 | 0.25 | 0.25 | 0.8979(14) | 0.030(3) | 0.034(4) | 0.034(4) | 0.021(6) | 0 | 0 | 0 |
| O6* | 0.6781(16) | 0.3367(18) | 0.4365(17) | 0.063(8) | 0.047(10) | 0.084(14) | 0.059(11) | 0.043(9) | 0.033(8) | 0.050(9) |
| O7* | 0.75 | 0.25 | 0.5 | 0.033(8) | 0.032(10) | 0.032(10) | 0.033(14) | 0 | 0 | 0 |

*O6 occupancy = 0.60(4); O7 occupancy = 0.60(6).

Table 5. Selected bond distances (Å) in favreauite.

| | | | |
|---|---|---|---|
| Pb | O4 | 2.553(5) | ×4 |
| | O2 | 2.772(6) | ×4 |
| Bi | O1 | 2.266(5) | ×4 |
| | O3 | 2.714(6) | ×4 |
| Se | O3 | 1.680(5) | |
| | O2 | 1.693(6) | |
| | O4 | 1.719(6) | |
| Cu1 | O1 | 1.961(6) | ×2 |
| | O3 | 1.957(5) | ×2 |
| | O6 | 2.461(13) | ×2 |
| Cu2 | O1 | 1.943(5) | |
| | O1 | 1.947(5) | |
| | O4 | 1.957(5) | |
| | O2 | 1.981(6) | |
| | O6 | 2.415(15) | |
| | O5 | 2.875(8) | |

from the carbon coating, but may also contain a contribution from minor C in the sample. However, no N $K$ peak was observed. Hence, it seems likely that some $CO_3^{2-}$ or $HCO_3^{-}$ is present in the O6/O7 cluster. Although no effervescence was observed when a favreauite crystal was treated with acid, this is not surprising, since the calculated $CO_2$ content for even the most carbon-rich hypothetical end-member $PbBiCu_6O_4(SeO_3)_4(HCO_3)\cdot H_2O$ is only 3.0 wt%.

We note that the planar triangular geometry of carbonate and nitrate groups is not compatible with placement of the cation at O7 and oxygens at the exact O6 positions. Furthermore, the $\bar{4}$ rotoinversion axis passing through O7 would require that in the long-range average structure, an $XO_3$ group ($X =$ C or N) show at least four-fold orientational disorder. Hence, the O6 site would actually be a superposition of several split sites of very low individual scattering factors: the minimum number of split sites per O6 would be three for equilateral triangular $CO_3^{2-}$ or $NO_3^{-}$ groups, but perhaps twelve for the less regular $HCO_3^{-}$. Site splitting is supported by the observation that the O6 thermal ellipsoids are remarkably large and anisotropic, being strongly elongated tangential to the O6–O7 vector (Fig. 4). Unfortunately, the very low site-scattering factors and large number of structural parameters render robust refinement of such complex splitting patterns impossible. Structure models were constructed in which all three oxygen atoms of a $CO_3^{2-}$ or $HCO_3^{-}$ group lay within 0.4 Å of an O6 site, but were not satisfactory in that oxygen bond valence sums tended to be low when the oxygen atoms were unprotonated, but high on protonated ones.

The weak Raman features noted above do not unambiguously identify the unanalysed species present. We compared them with Raman and infrared data for

Table 6. Bond-valence analysis for favreauite, omitting very weak bonding to the O7 site (discussed in text). Values are expressed in valence units.

| | Pb | Bi | Cu1 | Cu2 | Se | Σ |
|---|---|---|---|---|---|---|
| O1 | | 0.56 × 4 ↓ | 0.47 ×2 ↓ | 0.49 + 0.48 | | 2.01 |
| O2 | 0.19 ×4 ↓ | | | 0.44 | 1.38 | 2.01 |
| O3 | | 0.22 ×4 ↓ | 0.47 ×2 ↓ | | 1.42 | 2.11 |
| O4 | 0.30 ×4 ↓ | | | 0.47 | 1.29 | 2.06 |
| O5 | | | | 0.04 ×4 → | | 0.16 |
| O6 | | | 0.12 ×2 × 0.6* ↓ | 0.14 ×1 × 0.6* ↓ | | 0.26 |
| Σ | 1.97 | 3.14 | 2.02 | 2.01 | 4.09 | |

*These multiplicities = (number of bonds to O6) × (O6 site occupancy).
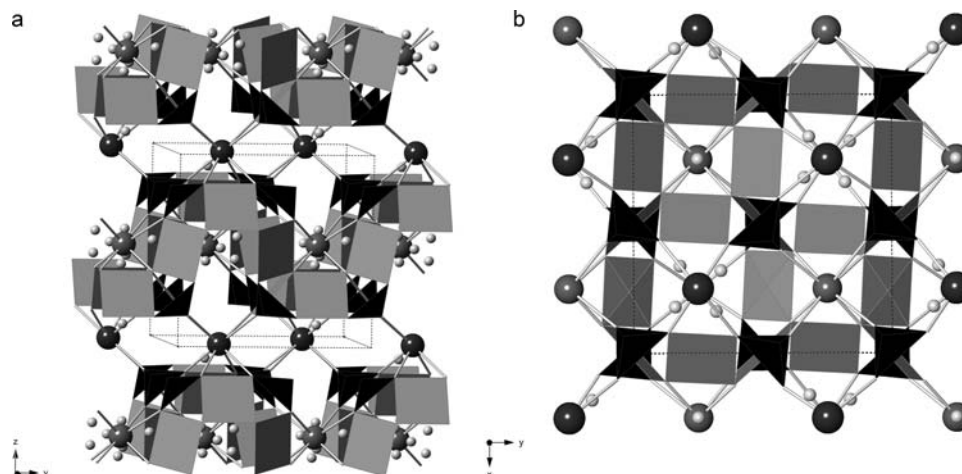
Fig. 2. Structure of favreauite, emphasising cation-centred polyhedra. Grey rectangles = $CuO_4$, black triangular pyramids = $SeO_3$, large dark grey spheres = Pb, smaller medium grey spheres = Bi, very small light grey spheres = O5 (at similar $z$ to Pb) and O6/O7 (tetrahedral groups at similar mean $z$ to Bi). (a) View approximately down **x**, highlighting highly corrugated Cu–O layers ∥ (001), branched by $SeO_3$ pyramids, and approximately face-centred cubic substructure of (Pb,Bi), with Bi in the hollows of the Cu–O layer and Pb between the layers. (b) View down **z**, showing rotational sense of the fourfold axis due to twisting of the Cu–O layer.
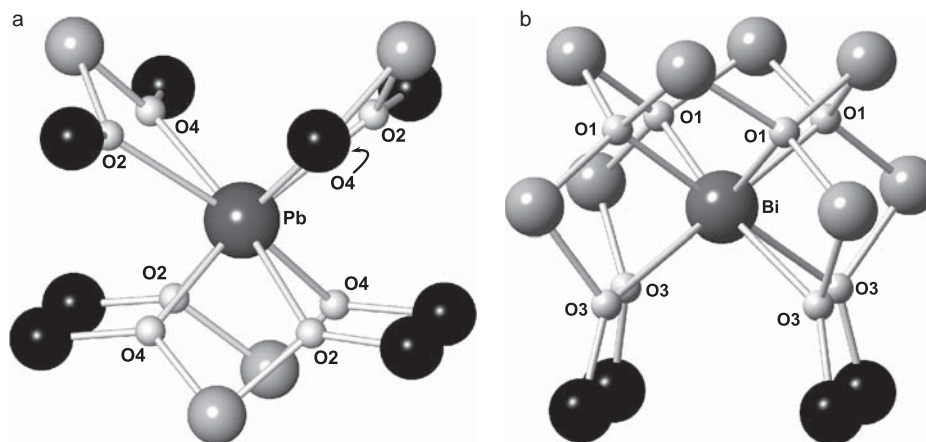


Fig. 3. Local environments of Pb and Bi (large grey spheres) in favreauite. Viewing direction is nearly down **x**, with **z** vertical. Oxygen ligands are small white spheres; next-nearest neighbour cations are Cu (light grey spheres) and Se (black). (a) Pb is surrounded by a tetrahedron of four O2 and an inverse tetrahedron of four O4 (one hidden behind Se), to give an overall point symmetry $\bar{4}$ at Pb, with no lone-pair steeroactivity. All oxygens are bound to one Pb, one Cu and one Se, and bond distances to Pb are relatively similar: Pb–O2 = 2.772 Å, Pb–O4 = 2.553 Å. (b) Bi, bonded to four O1 on one side and four O3 on the other, giving polar point symmetry 4 at Bi. O1 is bonded to 3 Cu, while O3 is bonded to 1 Cu + 1 Se. The bond distances to Bi are very different: Bi–O1 = 2.266 Å, Bi–O3 = 2.714 Å, implying that the Bi lone pair is directed in the –**z** direction.

carbonate and bicarbonate in minerals and in solution from Huang & Kerr (1960); Davis & Oliver (1972); Nyquist *et al.* (1996) and Frantz (1998), and data for nitrates from Akiyama *et al.* (1980); Nyquist *et al.* (1996) and Frost *et al.* (2004, 2005). The band at 1065 $cm^{-1}$ may be the $\nu_1$ symmetric stretch of either $CO_3^{2-}$ or $NO_3^{-}$. The 1341 $cm^{-1}$ band is too low in frequency to be from $CO_3^{2-}$ but could be $\nu_3$ of $NO_3^{-}$ or $HCO_3^{-}$. The 989 $cm^{-1}$ band is unusually low in frequency for any of these species, but this and the 1341 $cm^{-1}$ band fall within the wavenumber ranges for $HCO_3^{-}$ observed by Frantz (1998) in high-temperature solutions.

The electron count of 4.8 $e^{-}$ at O6 corresponds to 0.6 of an oxygen at each of four O6 sites, or 0.8 of an oxygen at each of three sites approximating the O6 positions. The 4.8 $e^{-}$ of scattering at O7 is equivalent to 0.8 of a carbon. Thus, the site scattering factors at O6 and at O7 and net overall charge of –1 could be simultaneously satisfied by a combination of $0.6[HCO_3^{-}] + 0.2[CO_3^{2-}]$ on the O6/O7 site complex, with no $OH^{-}$ or $H_2O$. However, this solution is
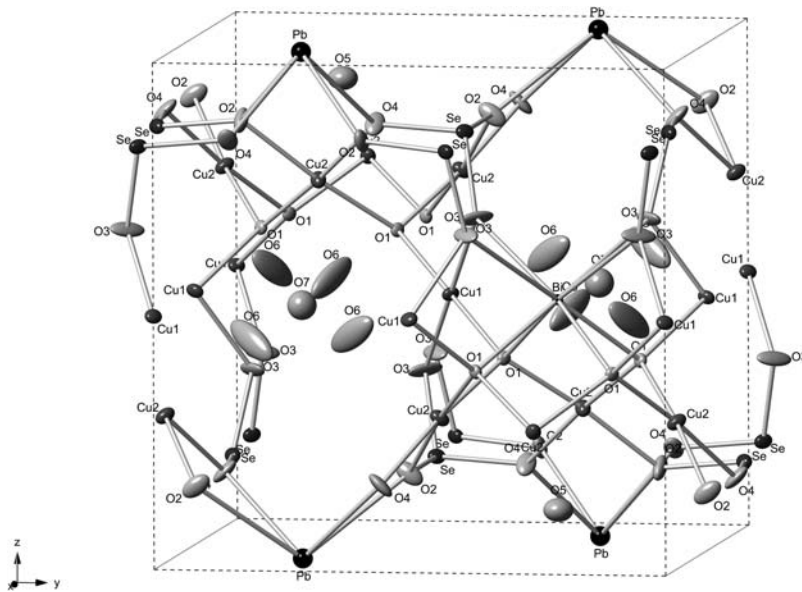
Fig. 4. Unit cell of favreauite showing 50 % thermal ellipsoids. Note very large, anisotropic ellipsoids for O6.
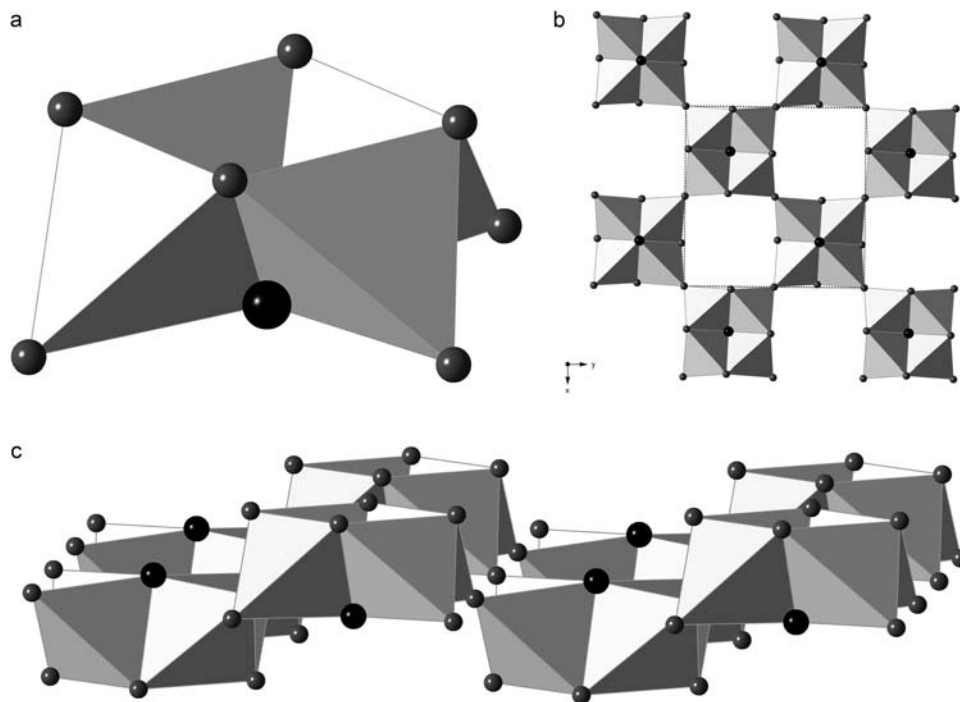


Fig. 5. (a) The ''half-cube'' cluster $Cu_8BiO_4$ of oxygen-centred tetrahedra in favreauite. Larger dark grey sphere is Bi; smaller, lighter grey spheres are Cu. (b) Edge-sharing of half-cubes to form a continuous layer $Cu_6BiO_4$ in favreauite, viewed down **z**. (c) Layer viewed nearly down **x**, to show corrugated pattern of half-cubes at two different heights.

not unique, and the estimated errors in quantification are large. Given the difficulty in identifying, quantifying and locating the light atoms present in the O6/O7 complex, we retain the simplest possible ideal formula for favreauite as $PbBiCu_6O_4(SeO_3)_4(OH)\cdot H_2O$, while acknowledging that the true situation is more complex, with unknown proportions of orientationally disordered, unidentified complex anions replacing the ''hydroxide''.

## 7.2. Relationship to other structures

The structure of favreauite is unique, but is very closely related to that of nabokoite, $KCu_7Te^{4+}O_4(SO_4)_5Cl$ ($P4/ncc$, $a = 9.833$ Å and $c = 20.591 = 2 \times 10.2955$ Å; Pertlik & Zemann, 1988). Atlasovite, $KCu_6Fe^{3+}BiO_4(SO_4)_5Cl$, is presumably isostructural with nabokoite since it has the same space group, similar unit-cell parameters and can form zones
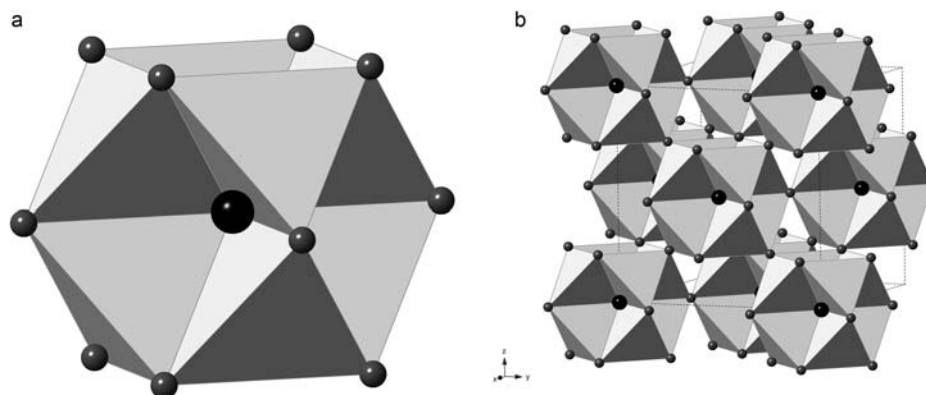
Fig. 6. (a) The ''cubic'' cluster $Cu_{12}PbO_8$ in murdochite. A cube of oxygen atoms lies at the centres of eight tetrahedra of cations. One Pb (dark sphere) at the centre of the cube is shared by all eight tetrahedra, while twelve Cu (light spheres) form a cuboctahedron surrounding the oxygen atoms. (b) Connection of murdochite cubes to make a three-dimensional framework $Cu_6PbO_8$; note that this can be described as fused layers with the same topology as those of Figure 5c.

within nabokoite crystals (Popova *et al.*, 1987). The similarity of favreauite and nabokoite is emphasised if the structure is described using oxygen-centred tetrahedra, an approach that has proven fruitful in the structural description of many compounds of cations such as $Cu^{2+}$, $Pb^{2+}$ and $Bi^{3+}$ with Lewis acid strength near 0.50 valence units (O'Keeffe & Hyde, 1985; Krivovichev *et al.*, 2013).

The anion-centred description of favreauite focusses on O1, which is tetrahedrally coordinated by 3Cu + 1Bi, while O2–O4 are in only three-fold coordination by Cu + Se + (Bi or Pb) and O5–O7 are only weakly bound to Cu. In favreauite, the $O1(Cu_3Bi)$ tetrahedra share edges in blocks of four to form a $Cu_8BiO_4$ cluster (Fig. 5a) which can be termed a ''half-cube'' for comparison with a related cubic cluster (below). Each half-cube shares only its four lower edges or four upper edges with neighbours, to form a corrugated $[Cu_6BiO_4]^{7+}$ layer in favreauite (Fig. 5b and c). The $[Cu_6TeO_4]^{8+}$ layer of nabokoite, and presumably $[Cu_6BiO_4]^{7+}$ of atlasovite, are topologically identical. The formulae of nabokoite and favreauite can be written to emphasise these layers as respectively $KCu[Cu_6TeO_4](SO_4)_4(SO_4)Cl$ and $Pb\square[Cu_6BiO_4](SeO_3)_4(OH)(H_2O)$, which shows that there is almost complete one-to-one correspondence between components of the two structures. The coordination environments of interlayer K and Pb are similar in their respective minerals; $S1O_4$ of nabokoite plays an analogous role to $SeO_3$ of favreauite; the disordered, roughly tetrahedral O6–O7 ''hydroxide'' moiety of favreauite corresponds to the $S2O_4$ tetrahedron in nabokoite, and Cl of nabokoite to O5 ($=H_2O$) of favreauite. Only the interlayer Cu2 site of nabokoite has no correspondent.

In order to accommodate the $SeO_3$ pyramids or $SO_4$ groups in these structures, there is a slight torsional distortion of the half-cubes, which breaks potential vertical mirror planes of symmetry; this twist in favreauite is very apparent in Figure 2b. The doubling of the nabokoite *c* repeat relative to that of favreauite is due to alternate layers having opposite senses of twist about the **z** axis.

Another closely related structure is that of $Pb_8O_5(PO_4)_2$ (Krivovichev & Burns, 2003) and its As analogue $Pb_8O_5(AsO_4)_2$ (Krivovichev *et al.*, 2004), which contains $Pb_9O_4$ half-cubes. Unlike the half-cubes of favreauite and nabokoite, these share their four lateral edges to form a $[Pb_7O_4]^{6+}$ layer that is planar rather than corrugated. Many other geometries of structural layer can be produced from edge-sharing $OM_4$ tetrahedra that do not form tetrameric half-cubes; examples are reviewed in Krivovichev *et al.* (2013).

The structures of favreauite, nabokoite (and presumably atlasovite) can be considered as derivatives of that of murdochite, $Cu^{2+}_6Pb^{4+}O_{8-x}(Cl,Br)_{2x}$, which has very similar unit-cell parameters to favreauite ($Fm\bar{3}m$, $a =$ 9.224 Å; Dubler *et al.* 1983). The oxygen atoms of murdochite all lie at the centres of $Cu_3Pb$ tetrahedra. Groups of eight tetrahedra in a cube-shaped pattern share edges to form $Cu_{12}PbO_8$ clusters (Fig. 6a), which are topologically similar to $Ca_{13}F_8$ portions of the fluorite structure, or two of the favreauite/nabokoite half-cubes joined back-to-back. The cubes are linked via Cu in <110> directions to form a three-dimensional framework in murdochite (Fig. 6b). Halide anions partly occupy the large voids that are surrounded by twelve cubes. An alternative view of the murdochite $Cu_6O_8$ framework is as a (4,3)-connected net, the ''twisted boracite'' or **tbo** net of Delgado-Friedrichs *et al.* (2006), with Cu in square-planar and O in triangular coordination. Pb occupies the smaller of two types of cage in this net, 8-coordinated by O, while (Cl,Br) is in the larger cages, 12-coordinated by Cu, playing a role analogous to the O6/O7 cluster of favreauite or $S2O_4$ in nabokoite.

The large $Pb^{4+}$ cations of murdochite form a face-centred cubic array. This is also the case for $(Pb^{2+}+Bi^{3+})$ in favreauite and $(K^++Te^{4+})$ in nabokoite, in both of which the two types of large cation alternate in layers || (001). Retention of this large cation array in the layered structures emphasises that the layers can be derived from the murdochite framework by if $Cu_{12}MO_8$

cubes are reduced to $Cu_8MO_4$ half-cubes through systematic omission of $Cu^{2+}$ and oxygen, and additional components such as $SeO_3^{2-}$ are introduced into the interlayer space thus formed.

The different distortion patterns of the Pb and Bi coordination polyhedra in favreauite are noteworthy. It is rare, but not unknown, for $Pb^{2+}$ to show a complete lack of lone-pair stereoactivity. Another mineralogical example is rosiaite, $Pb_2Sb_2O_6$ (Basso *et al.*, 1996) with the $Li_2ZrF_6$ structure, in which the six Pb–O distances are symmetrically constrained to be equal and in a nearly regular octahedral configuration ($\bar{3}$ point symmetry). There, the Pb–O bond valence cannot depart significantly from the average value of $^1/_3$ because each oxygen atom is also bonded strongly to two $Sb^{5+}$ (bond valence necessarily close to $^5/_6$). Similar topological/bond-valence limitation of lone-pair stereoactivity may result in quite different degrees of asymmetry even for $PbO_n$ polyhedra in the same structure. Note the difference between relatively symmetrical $Pb1O_8$ and asymmetrical $Pb2O_7$ in $Pb_3Fe^{3+}{}_2(PO_4)_4(H_2O)$ (Mills *et al.*, 2010), and the relatively inactive lone pairs of Pb3 in housleyite (Kampf *et al.*, 2010) and Pb1 in the schieffelinite structure (Kampf *et al.*, 2012b). This behaviour also occurs for smaller and more electronegative lone-pair cations such as $Te^{4+}$. Christy & Mills (2013) quantified lone-pair stereoactivity for $Te^{4+}O_6$ polyhedra using the separation between Te and the centre of the sphere of best fit of the oxygen coordination polyhedron (equated with the centre of lone-pair electron density), and obtained very different distances (1.04 and 1.43 Å) for Te1 and Te2 in juabite (Burns *et al.*, 2000).

In favreauite, both oxygen atoms in the Pb coordination shell (O2 and O4) are also bonded strongly to Cu2 (bond valence 0.44 and 0.47 *v.u.* respectively; Table 6) and Se (bond valences 1.41 and 1.25), which again provides a topological restriction on the Pb–O bond valence to a narrow range around the mean value of ¼ (Pb–O2 = 0.19 and Pb–O4 = 0.30 *v.u.*), thus inhibiting lone-pair stereoactivity and facilitating occupation of a site with non-polar point symmetry. Conversely, the two oxygen atoms that are bonded to Bi have quite different coordination environments, requiring significantly different Bi–O bond valences and distances. O1 is bonded to Cu1 + 2 Cu2, as well as making a bond of 0.56 *v.u.* to Bi, whereas O3 bonds to Cu1 + Se, with a bond of 0.22 *v.u.* to Bi (Table 6). Although $Pb^{2+}$ and $Bi^{3+}$ frequently substitute for one another in crystal structures, the existence in the favreauite structure of two sites of appropriate size, one intrinsically of non-polar symmetry while the other is polar, is sufficient to drive ordering between $Pb^{2+}$ and $Bi^{3+}$. The $Pb^{2+}$, which is larger, less electronegative and less prone to lone-pair stereoactivity, enters the non-polar site, while $Bi^{3+}$, which shows the converse properties, goes into the polar site. The availability of two different large cations is probably essential to formation of a favreauite-like structure. A cation with a highly stereoactive lone pair stabilises the cuprate layer ($Bi^{3+}$ in favreauite and atlasovite, $Te^{4+}$ in

nabokoite), while the interlayer cation either has no lone pair ($K^+$ in nabokoite and atlasovite) or a lone pair whose stereoactivity is suppressed ($Pb^{2+}$ in favreauite).

The structures of favreauite, nabokoite and presumably atlasovite currently provide the only known mineralogical examples of cuprate layers derived by deletion of atoms from the murdochite framework as described above. Indeed, murdochite itself is the only natural exemplar of its structure type. Searching the Inorganic Crystal Structure Database revealed only a small number of additional phases that are near-isotypic to murdochite: $Tl^{3+}Pd^{2+}{}_6O_8Tl^{1+}$ (Müller *et al.*, 1978), $Cu^{2.24+}{}_{1.6}Cu^{2.24+}{}_6O_8(Cl,NO_3)$ (Hayakawa *et al.*, 1991) and $Y^{3+}Cu^{2.33+}{}_6O_8Cl$ (Zouganelis *et al.*, 1991). Compounds have also been prepared with $In^{3+}$ or $Sc^{3+}$ replacing $Y^{3+}$ in the latter phase (Bushida *et al.*, 1991). All of these have square-planar coordinated $d^9$ $Cu^{2+}$ or low-spin $d^8$ $Cu^{3+}$ or $Pd^{2+}$ as the framework cation. The 8-fold coordinated interstitial site contains relatively highly charged cations ($Sc^{3+}$, $Y^{3+}$, $In^{3+}$, $Tl^{3+}$, $Pb^{4+}$ or $Cu^{2-3+}{}_{1-2}$), and the large cage contains either anions or large, low-charge cations ($Cl^-$, $NO_3^-$ or $Tl^+$), usually split over several off-centre positions. The diversity of large cations and cage-filling species found in these compounds suggests that other members of the nabokoite-favreauite supergroup may yet be discovered.

# References

Akiyama, K., Morioka, Y., Nakagawa, I. (1980): Raman and infrared spectra and lattice vibrations of $KNO_3$ crystal. *J. Phys. Soc. Japan*, **48**, 898–905.

Basso, R., Lucchetti, G., Zefiro, L., Palenzona, A. (1996): Rosiaite, $PbSb_2O_6$, a new mineral from the Cetine mine, Siena, Italy. *Eur. J. Mineral.*, **8**, 487–492.

Brugger, J., Meisser, N., Krivovichev, S., Armbruster, T., Favreau, G. (2007): Mineralogy and crystal structure of bouazzerite from Bou Azzer, Anti-Atlas, Morocco: Bi–As–Fe nanoclusters containing $Fe^{3+}$ in trigonal prismatic coordination. *Am. Mineral.*, **92**, 1630–1639.

Burla, M.C., Caliandro, R., Camalli, M., Carrozzini, B., Cascarano, G.L., De Caro, L., Giacovazzo, C., Polidori, G., Spagna, R. (2005): SIR2004: an improved tool for crystal structure determination and refinement. *J. Appl. Cryst.*, **38**, 381–388.

Burns, P.C., Clark, C.M., Gault, R.A. (2000): Juabite, $CaCu_{10}(Te^{4+}O_3)_4(AsO_4)_4(OH)_2(H_2O)_4$: crystal structure and revision of the chemical formula. *Can. Mineral.*, **38**, 809–816.

Bushida, K., Yazawa, I., Zouganelis, G., Conard, T., Terada, N., Kaneko, K., Hirabayashi, M., Ihara, H. (1991): Synthesis and properties of new cubic $Cu_6O_8.MX$ compounds as a candidate of cubic copper oxide superconductors. *Physica C*, **185–189**, 2727–2728.

Christy, A.G. & Mills, S.J. (2013): Effect of lone-pair stereoactivity on polyhedral volume and structural flexibility: application to $Te^{IV}O_6$ octahedra. *Acta Cryst.*, **B69**, 446–456.

Davis, A.R. & Oliver, B.G. (1972): A vibrational spectroscopic study of the species present in the $CO_2$–$H_2O$ system. *J. Solution Chem.*, **1**, 329–339.

Delgado-Friedrichs, O., O'Keeffe, M., Yaghi, O.M. (2006): Three-periodic nets and tilings: edge-transitive binodal structures. *Acta Cryst.*, **A62**, 350–355.

Dubler, E., Vedani, A., Oswald, H.R. (1983): New structure determination of murdochite, $Cu_6PbO_8$. *Acta Cryst.*, **C39**, 1143–1146.

Frantz, J.D. (1998): Raman spectra of potassium carbonate and bicarbonate aqueous fluids at elevated temperatures and pressures: comparison with theoretical simulations. *Chem. Geol.*, **152**, 211–225.

Frost, R.L., Leverett, P., Williams, P.A., Weier, M.L., Ericksson, K.L. (2004): Raman spectroscopy of gerhardtite at 298 and 77 K. *J. Raman Spectrosc.*, **35**, 991–996.

Frost, R.L., Ericksson, K.L., Weier, M.L., Leverett, P., Williams, P.A. (2005): Raman spectroscopy of likasite at 298 and 77 K. *Spectrochim. Acta A*, **61**, 607–612.

Grundmann, G., Lehrberger, G., Schnorrer-Köhler, G. (1990): The El Dragón mine, Potosí, Bolivia. *Mineral. Rec.*, **21**, 133–150.

Hayakawa, H., Akiba, E., Ihara, H., Ono, S. (1991): Crystal structure of new compounds, $Cu_6O_8Cu_2X$ ($X=$ Cl, $NO_3$). *Jap. J. Appl. Phys.*, **30**, 1303–1306.

Huang, C.K. & Kerr, P.F. (1960): Infrared study of the carbonate minerals. *Am. Mineral.*, **45**, 311–324.

Kampf, A.R. & Favreau, G. (2004): Jacquesdietrichite, $Cu_2[BO(OH)_2](OH)_3$, a new mineral from the Tachgagalt mine, Morocco: Description and crystal structure. *Eur. J. Mineral.*, **16**, 361–366.

Kampf, A.R., Marty, J., Thorne, B. (2010): Lead-tellurium oxysalts from Otto Mountain near Baker, California: II. Housleyite, $Pb_6CuTe_4O_{18}(OH)_2$, a new mineral with Cu-Te octahedral sheets. *Am. Mineral.*, **95**, 1337–1342.

Kampf, A.R., Mills, S.J., Rossman, G.R., Steele, I.M., Pluth, J.J., Favreau, G. (2011): Afmite, $Al_3(OH)_4(H_2O)_3(PO_4)(PO_3OH) \cdot H_2O$, a new mineral from Fumade, Tarn, France: description and crystal structure. *Eur. J. Mineral.*, **23**, 269–277.

Kampf, A.R., Mills, S.J., Housley, R.M., Favreau, G., Boulliard, J.C., Bourgoin, V. (2012a): Angarfite, $NaFe^{3+}_5(PO_4)_4(OH)_4 \cdot 4H_2O$, a new mineral species from the Angarf-Sud Pegmatite,

Morocco: description and crystal structure. *Can. Mineral.*, **50**, 781–791.

Kampf, A.R., Mills, S.J., Housley, R.M., Rumsey, M.S., Spratt, J. (2012b): Lead-tellurium oxysalts from Otto Mountain near Baker, California: VII. Chromschieffelinite, $Pb_{10}Te_6O_{20}(OH)_{14}(CrO_4)(H_2O)_5$, the chromate analog of schieffelinite. *Am. Mineral.*, **97**, 212–219.

Krivovichev, S.V. & Burns, P.C. (2003): Crystal chemistry of lead oxide phosphates: crystal structures of $Pb_4O(PO_4)_2$, $Pb_8O_5(PO_4)_2$ and $Pb_{10}(PO_4)_6O$. *Z. Krist.*, **218**, 357–365.

Krivovichev, S.V., Armbruster, T., Depmeier, W. (2004): Crystal structures of $Pb_8O_5(AsO_4)_2$ and $Pb_5O_4(CrO_4)$, and review of PbO-related structural units in inorganic compounds. *J. Solid State Chem.*, **177**, 1321–1332.

Krivovichev, S.V., Mentré, O., Siidra, O.I., Colmont, M., Filatov, S.K. (2013): Anion-centred tetrahedra in inorganic compounds. *Chem. Rev.*, **113**, 6459–6535.

Meisser, N., Brugger, J., Krivovichev, S., Armbruster, T., Favreau, G. (2012): Description and crystal structure of maghrebite, $MgAl_2(AsO_4)_2(OH)_2 \cdot 8H_2O$, from Aghbar, Anti-Atlas, Morocco: first arsenate in the laueite mineral group. *Eur. J. Mineral.*, **24**, 717–726.

Mills, S.J., Kolitsch, U., Miyawaki, R., Hatert, F., Poirier, G., Kampf, A.R., Matsubara, S., Tillmanns, E. (2010): $Pb_3Fe^{3+}_2(PO_4)_4(H_2O)$, a new octahedral-tetrahedral framework structure with double-strand chains. *Eur. J. Mineral.*, **22**, 595–604.

Mills, S.J., Rumsey, M.S., Favreau, G., Spratt, J., Raudsepp, M., Dini, M. (2011): Bariopharmacoalumite, a new mineral species from Cap Garonne, France and Mina Grande, Chile. *Mineral. Mag.*, **75**, 135–144.

Mills, S.J., Kampf, A.R., Housley, R.M., Favreau, G., Pasero, M., Biagioni, C., Merlino, S., Berbain, C., Orlandi, P. (2012a): Omsite, $(Ni,Cu)_2Fe^{3+}(OH)_6[Sb(OH)_6]$, a new member of the cualstibite group from Oms, France. *Mineral. Mag.*, **76**, 1347–1354.

Mills, S.J., Kampf, A.R., McDonald, A.M., Favreau, G., Chiappero, P.J. (2012b): Forêtite, a new secondary arsenate mineral from the Cap Garonne mine, France. *Mineral. Mag.*, **76**, 769–775.

Müller, M., Thiele, G., Zöllner, C. (1978): Strukturparameter von $TlPd_3O_4$ aus einem Neutronen-Pulverdiagramm. *Zeitschr. Anorg. Allg. Chemie*, **443**, 19–22.

Nyquist, R.A., Kagel, R.O., Putzig, C.L., Leugers, M.A. (1996): Handbook of infrared and Raman spectra of inroganic compounds and organic salts. Academic Press, New York, 1184 p.

O'Keeffe, M. & Hyde, B.G. (1985): An alternative approach to nonmolecular crystal structures with emphasis on the arrangements of cations. *Struct. Bond*, **61**, 77–160.

Paar, W.H., Cooper, M.A., Moëlo, Y., Stanley, C.J., Putz, H., Topa, D., Roberts, A.C., Stirling, J., Raith, J.G., Rowe, R. (2012): Eldragónite, $Cu_6BiSe_4(Se_2)$, a new mineral species from the El Dragón mine, Potosí, Bolivia, and its crystal structure. *Can. Mineral.*, **50**, 281–294.

Pertlik, F. & Zemann, J. (1988): The crystal structure of nabokoite, $Cu_7TeO_4(SO_4)_5KCl$: the first example of a $Te^{IV}O_4$ pyramid with exactly tetragonal symmetry. *Miner. Petrol.*, **38**, 291–298.

Popova, V.I., Popov, N.S., Rudashevskiy, S.F., Polyakov, V.O., Bushmakin, A.F. (1987): Nabokoite $Cu_7TeO_4(SO_4)_5 \cdot KCl$ and atlasovite $Cu_6Fe^{3+}Bi^{3+}O_4(SO_4)_5 \cdot KCl$. New minerals of volcanic exhalations. *Zap. Vses. Mineral. Obshch.*, **116**, 358–367. [in Russian with English abstract]

Sarp, H. & Cerny, R. (1998): Description and crystal structure of yvonite, $Cu(AsO_3OH) \cdot 2H_2O$. *Am. Mineral.*, **83**, 383–389.

Sheldrick, G.M. (2008): A short history of *SHELX. Acta Cryst.*, **A64**, 112–122.

Topa, D., Makovicky, E., Favreau, G., Bourgoin, V., Boulliard, J.C., Zagler, G., Putz, H. (2013): Jasrouxite, a new Pb–Ag–As–Sb member of the lillianite homologous series from Jas Roux, Hautes-Alpes, France. *Eur. J. Mineral.*, **25**, 1031–1038.

Verma, V.P. (1999): A review of synthetic, thermoanalytical, IR, Raman and X-ray studies on metal selenites. *Thermochim. Acta*, **327**, 63–102.

Zouganelis, G., Bushida, K.I., Yazawa, I., Terada, N., Jo, M., Hayakawa, H., Ihara, H. (1991): Structure refinement of the $Cu_6O_8.YCl$ compound. *Solid State Comm.*, **80**, 709–713.